HiSST: 2nd International Conference on
High-Speed Vehicle Science Technology
11–15 September 2022, Bruges, Belgium

Numerical Investigation of Different Ramp Models and Length on Shock Wave Boundary Layer Interactions

Fatmanur Aleyna ÖZCAN[1], Muhammed Osama BALKHI[2] Ahmet Selim DURNA[3]

Abstract

Shock-wave boundary layer interaction is therefore a spectacle commonly associated with aerospace devices when a shock wave meets a boundary layer in high-speed flows. In this study, the effect of different ramp lengths at three different ramp angles of 24º, 33º, and 50º, respectively, at M=2.52 will be examined. Investigations were performed with a commercial Computational Fluid Dynamics software based on two different ramp angle geometries with Schlieren images. The results obtained are compatible with the experimental results. The separation shock's angle is independent of ramp angle and length. Separation width increases with ramp angle and length. The separation shock's strength increases with ramp angle, however reattachment shock's strength almost stays constant.

Keywords: shock wave boundary layer interaction, ramp length effect, compression ramp

[1] *Graduate student researcher, RWTH Aachen University, aleyna.oezcan@rwth-aachen.de*
[2] *Graduate student researcher , Istanbul Technical University, mosamabalkhi@gmail.com*
[3] *Assistant Professor, University of Samsun, ahmetselim.durna@samsun.edu.tr*

1. Introduction

Shock-wave boundary layer interaction (SWBLI) is therefore a spectacle commonly associated with aerospace devices when a shock wave meets a boundary layer in high-speed flows. Thus, an in-depth understanding of the boundary layer phenomena is essential for efficient aerodynamic and propulsion design. Nevertheless, some observations have not been satisfactorily explained yet and physical processes have been poorly understood. Therefore, SWBLI has been studied for nearly 80 years for their omnipresence in high-speed flight and their influence on vehicle and component performance [1]. The study of SWBLI has been a matter of interest in the aerospace community since Ferri's first investigations of the phenomenon in 1940 [2]. Since no theoretical solution for this problem has been conceived, experimental and computational resources has been driven on SWBLI to study the structure and dynamics in detail, which have been examined in several review articles continue to supply further understanding on the spectacle, and to support modern computational and turbulence modeling efforts [3][4][5][6][7].

Verma et al. [8] reported an experiment on a 24º compression ramp at M=2.05, where the incoming boundary-layer thickness was 3.85 mm. The interaction length of the SWBLI in Ref. [8] which measured by Coloured Schlieren Technique was about 20 mm. Similarly, with Verma et al. but with adding different ramp angles, Sun [7] has been experimentally studied the flow structures of SWBLI at six compression ramps with angles ranging from 20º to 30º with an interval of 2º at M=2.0 to reveal the effect of the ramp angle by high-speed Schlieren imaging technique. The interaction length of the 24º compression ramp SWBLI at M=2.05 has been found similar with the report of Verma et al. [8]. Sun has been reported that increasing the ramp angle α, while keeping the ramp height *h* equal, unhurriedly moves the separation shock wave upstream. Also, in all the SWBLIs the separation shock waves in the Schlieren analysis, has been reported by Sun with a similar angle of 47º. Recently, similar to Sun [7], Ramaswamy and Schreyer [9] have been experimentally studied with the compression ramp angles of 24° and 33°at a freestream Mach number of M=2.52 by using oil-flow and focusing-schlieren visualizations and 2C particle image velocimetry (PIV). Ramaswamy and Schreyer have been observed by PIV that the 37° compression-ramp, shows a larger separation bubble than the 24° compression-ramp interaction and the separation shock angle for both compression-ramp interactions have been remained nearly constant, with a value of 33°. In the Schlieren analysis, the separation shock angle for both compression-ramp interactions have been nearly similar and has been found to be equal to 33°which is marginally smaller than PIV estimations.

Experimental investigations of the compression ramp angle effect on SWBLI structures have been a reference for several numerical inquisitions. Zheltovodo's [10] experiments at M=3 have been utilized for a sequel of simulation validations. Direct numerical DNS simulation by Hickel et al., [11] 24º compression ramp at M=2.9, and the results of LES simulation at 25° compression ramp at M=2.88 by Adams et al. [16], can be cited as examples of similar important studies that reference Zheltovodo's experiments.[13].In addition, as one of the other important studies, numerical investigations of Rizzetta et al. [14] with more different ramp angles corresponding to experiments of Smiths and Muck [15] has been carried out at M=3.0 for the compression ramp angles of 8º, 16º, 20º and 24º performed by LES however, studies has been poorly predicted the experiment in all cases. Despite of previous less converging numerical studies with the experimental results, one of the best reference studies among today's studies that can reach parallel results with experimental results is numerical investigations of Zheltovodov et al. [12] with the compression ramp angle of 25°at a freestream Mach number of M=2.95 by LES simulations which has been a direct comparison of the experimental studies of a supersonic turbulent flow over a compression corner at different Mach numbers and deflection angles of Stolz et al. [16].Studies has been successfully confirmed in the terms of mean quantities such as shock position, separation and reattachment location, surface pressure distributions and turbulence structure at the exact ramp angle and Mach number.

The objective of the present paper is to investigate the effect of ramp length along with ramp angle. In this study, different compression ramp angles (namely 24°, 33°, and 50°) at a freestream Mach number of M=2.52 has been numerically studied.

2. Numerical Method

2.1. Geometry and Numerical Domain

The single compression ramp geometry was introduced to an appropriate domain as shown in the upper side of Figure 1. This demonstrates the geometry of the 24º ramp used in reference [9]. Nine different ramp models were created in total by varying both the ramp turning angle and length as showed in Table 1.

Table 1. Ramp models nomenclature

Turning angle / Ramp length [mm]	24°	33°	50°
20	A24-L20	A33-L20	A50-L20
39.4	A24-L39	A33-L39	A50-L39
100	A24-L100	A33-L100	A50-L100

Figure 1 also shows the structure grid of the domain for the ramp model A24-L39. This grid structure was composed using the ICEM CFD meshing tool. To model the boundary layer, a value of unity or less was set for the y^+ parameter and the first layer thickness was calculated accordingly to be found roughly as $1x10^{-6}$ m. A total 450,000 number of cells were created. Moreover, although a maximum aspect ratio of 776 was obtained in the boundary layer, almost perfect square elements were obtained on the rest of the domain.

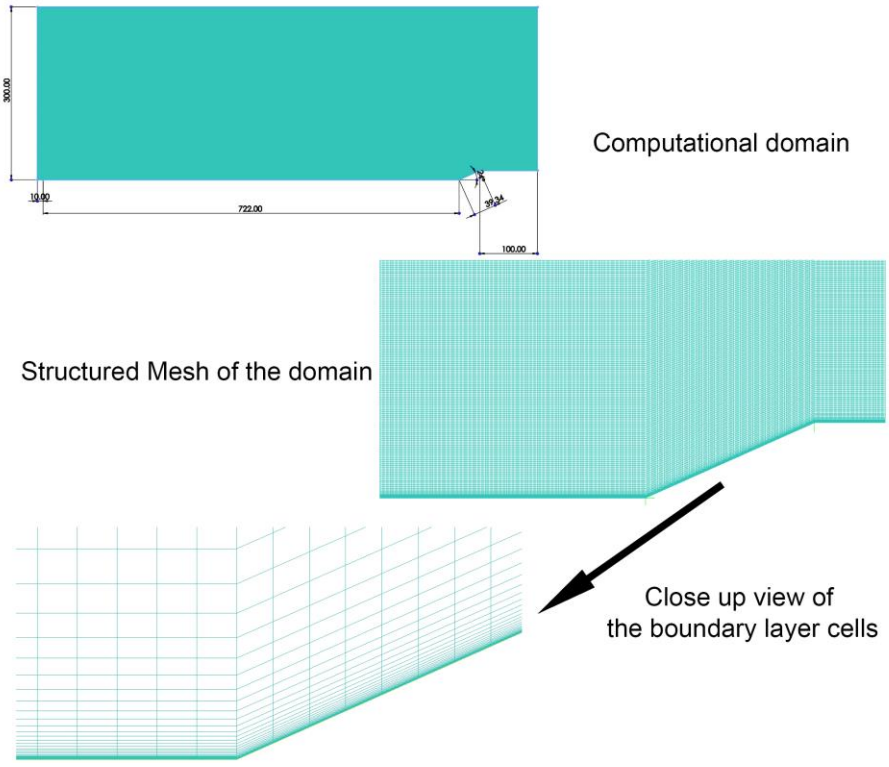

Fig 1. Computational domain and structure mesh of the domain and the ramp (A24-L39)

2.2. Boundary Conditions and Numerical Details

A freestream condition of M=2.52 and a total pressure of 56446.27 Pa were applied to the left and upper ends of the domain. Symmetry boundary condition was applied to a 0.01 m portion of the lower surface and a no-slip condition was applied to the remaining part of the bottom surface. Lastly, a zero-pressure gradient was applied to the right side of the domain. These conditions were adapted from [9] for validation and to investigate the case further.
A commercial Navier-Stokes solver (ANSYS Fluent) was used to simulate the $k-\omega$ turbulence model. A density-based, steady, and compressible flow was solved as well as a second order discretization for the pressure-velocity coupling.

2.3. Grid Independency

To investigate the dependency of the solutions on the grid, additional two mesh sizes were adapted by refining the mesh and were obtained by halving and doubling the cell numbers. For all the three meshes, cell aspect ratio and grid structure were kept nearly identical. A total number of 0.25M, 0.45M, and 0.75M cells are achieved for the coarse, medium and fine size meshes, respectively. Figure 2 shows the static pressure (non-dimensionalised with freestream static pressure) along the ramp wall for all the mesh sizes. It is observed that although the pressure values stay almost matching for the three sizes of mesh, the coarse mesh pressure values vary on the peak pressure point (X=0.75 m). Thus, the results mesh independent and the analysis will be carried out using the medium-sized mesh.

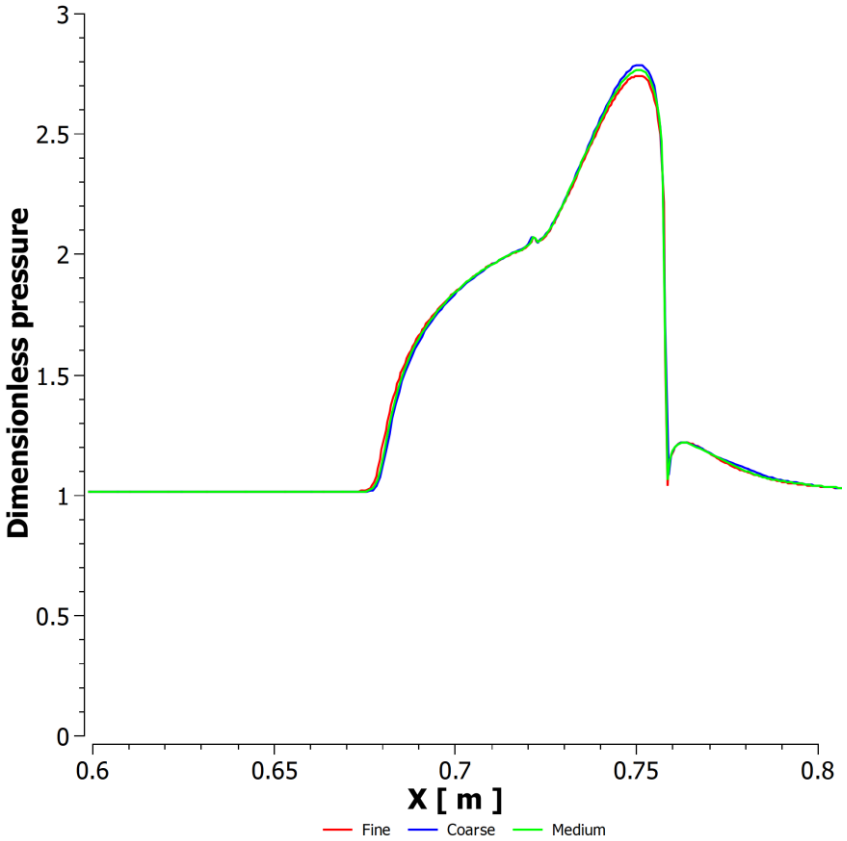

Fig 2. Static pressure (non-dimensionalised with freestream static pressure) along the ramp wall for three mesh sizes

3. Results and Discussion

3.1. Validation

Figure 3 shows a comparison of the averaged focusing-schlieren image of the 24° and 33° ramp models [9] and the CFD results of this study (Mach number contour). The shock wave separation angle, namely 33° for this case [9], was obtained with the CFD technics, and a similarity of the flow pattern was remarked.

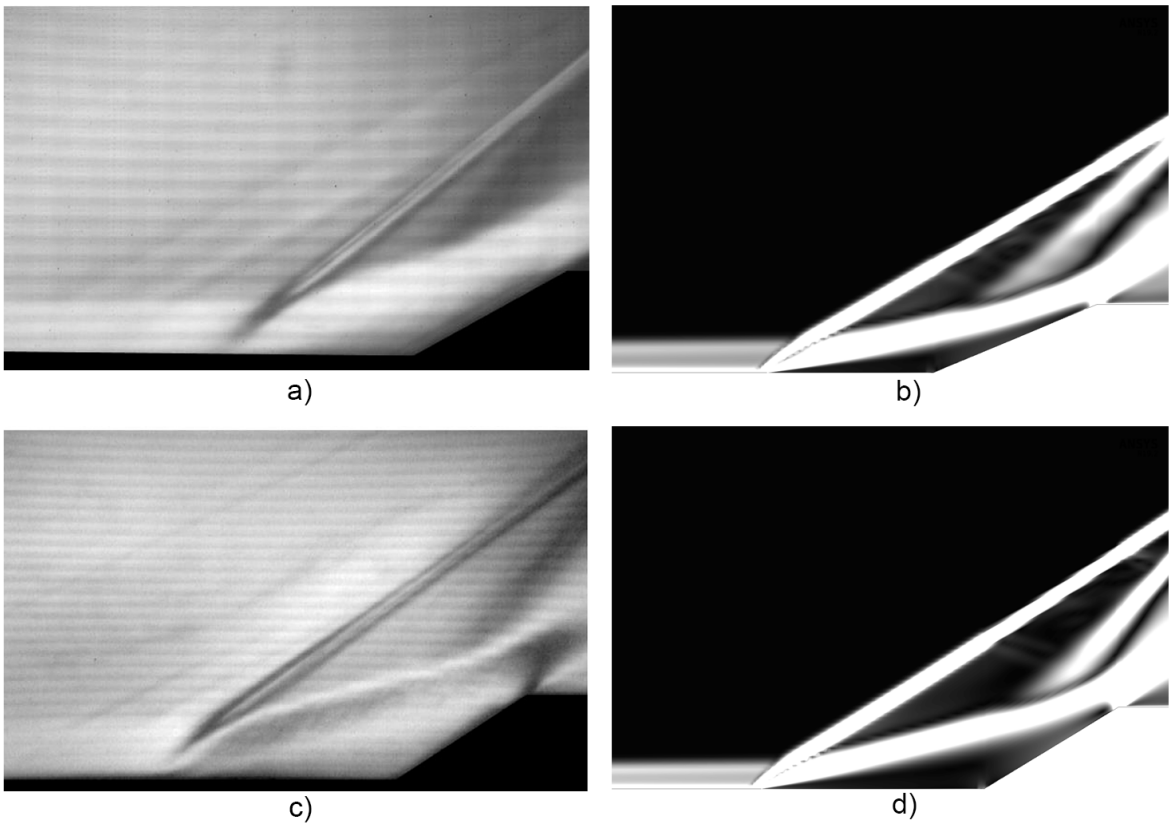

Fig 3. a) 24° c) 33° ramp model Averaged focusing-schlieren [9] b) 24° d) 33° ramp model CFD results of this study

3.2. Results

Figure 4 shows the Mach contour of the examined nine ramp models where ramp angle and length increase horizontally and vertically, respectively. It is remarked that for matching ramp angles and increasing length the region under the shear layer enlarges. For all studied cases, the separation angle is observed to be almost identical. (Except for A50-L100) However, the Mach number behind the separation shock decreases with increasing ramp angle. Moreover, a similar observation is noticed for larger (increasing) ramp lengths.
Additionally, the Mach number of the region behind the reattachment shock is seen to be less for larger ramp angles and lengths. This might be an indicator of a stronger reattachment shock for these cases.

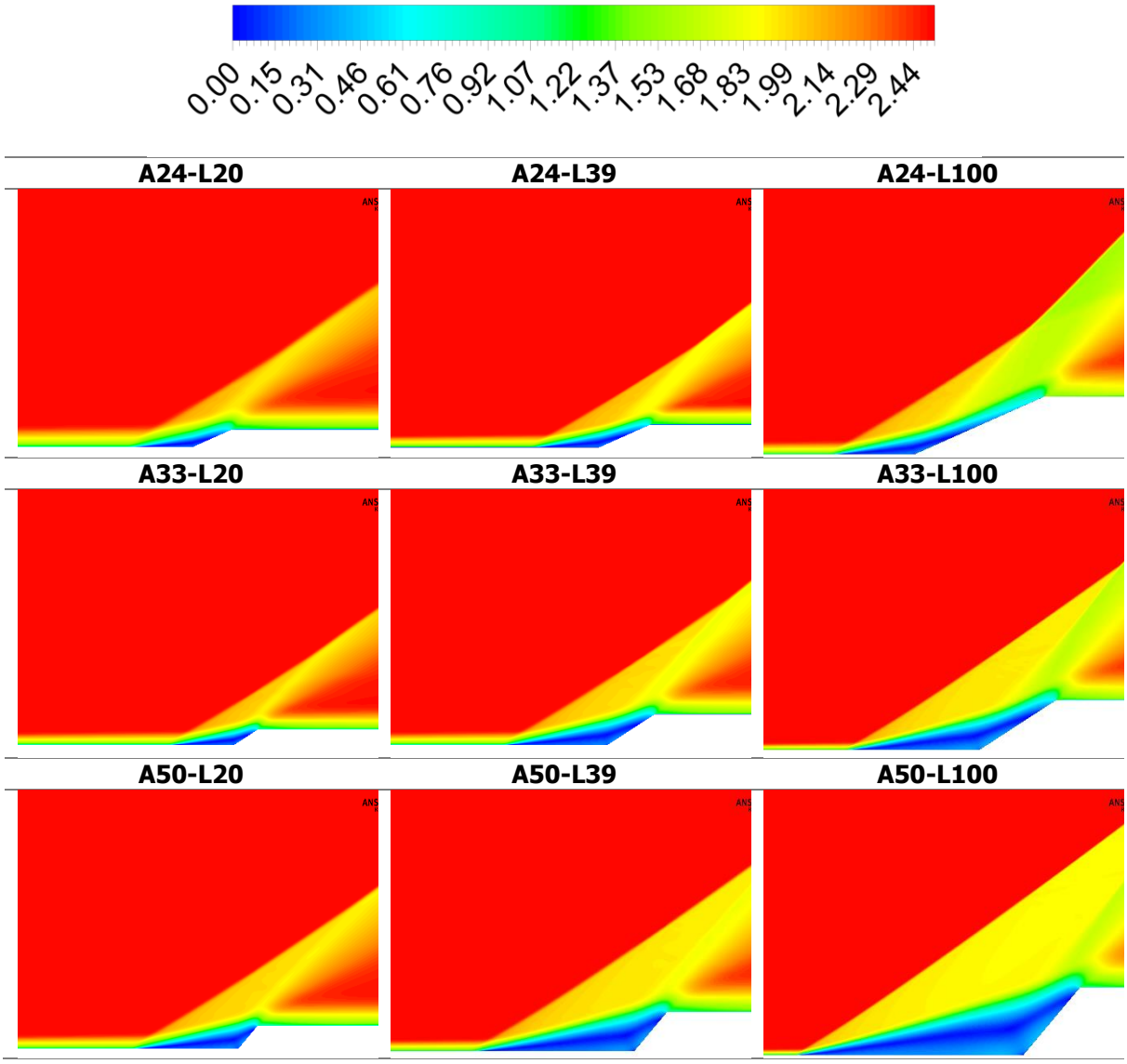

Fig 4. Mach number Contours for the nine ramp models

The separation shock angle, separation zone width, and strength of the separation and reattachment shocks for the studied ramp models are given in table one. All cases were solved using Standard $k-\omega$ (2 equations) turbulence model. ϑ is defined as the separation angle and $\boldsymbol{x/\delta}$ is the separation zone width measured from the compression corner divided by the boundary layer thickness. $\boldsymbol{\Psi}$ and $\boldsymbol{\xi}$ are described as the static pressure behind the separation and reattachment shocks, respectively, divided by the pressure values before passing through that shock.

For increasing ramp angles the separation shock angle ϑ stays constant with a value of 33°. A similar observation is noticed for increasing ramp length as the value of ϑ does not change for larger ramp lengths. However, a slight increment in ϑ (36°) is noticed for case A50-L100. This is interpreted by the large separation area affecting the relative regions or the large ramp angle/length.

For a constant ramp length, the separation zone width $\boldsymbol{x/\delta}$ is found to increase as the ramp angle increases. A relative remark is also noticed as $\boldsymbol{x/\delta}$ increases when the ramp angle is constant and the ramp length increases. As the ramp length is fixed the separation shock strength $\boldsymbol{\Psi}$ increases with ramp angle. This can also be stated for fixed ramp lengths and higher ramp lengths. The reattachment shock strength $\boldsymbol{\xi}$ increases remarkably for constant ramp angles as the length increases. However, interestingly, $\boldsymbol{\xi}$ values stay relatively close for fixed ramp lengths, even when the ramp angle show difference.

Table 1. Shock characteristics for different ramp models

	ϑ	x/δ	Ψ	ξ		ϑ	x/δ	Ψ	ξ		ϑ	x/δ	Ψ	ξ
A24-L20	33°	2.86	1.82	1.17	**A33-L20**	33°	4.47	1.84	1.16	**A50-L20**	33°	6.98	2	1.12
A24-L39	33°	4.69	1.86	1.23	**A33-L39**	33°	7.31	1.98	1.31	**A50-L39**	33°	12.45	2.1	1.18
A24-L100	33°	5.84	1.92	1.32	**A33-L100**	34°	14.35	2.13	1.33	**A50-L100**	36°	26.36	2.28	1.33

4. Conclusion

In this study, the effect of the separation shock angle, the separation zone width, and the SWBLI structures has been studied. Parameters such as shock strength and separation angle have been observed using two turbulence models. A validation study has given consistent results with the Schlieren Images. The results given in the following order were obtained: -Each case has been solved using Standard $k-\omega$ turbulence model. There has been no sparkly difference observed by changing the turbulence model. -The separation shock angle stays constant for increasing the ramp angle or length separately, or mutually. -The separation width increases by increasing the ramp angle or either by increasing the ramp length while keeping the ramp angle the same. (The separation area width increases by increasing the ramp angle or length while keeping the other parameter constant). - The strength of the shock increases by increasing the ramp angle or either by increasing the ramp length while keeping the ramp angle the same. -The power of the reattachment shock stays nearly the same by increasing the ramp angle but increases parallelly with the increase of the ramp length. In future studies, more experiments to research the effect of the ramp length are aimed. Also, more comprehensive turbulence models such as DNS instead of RANS are future options to improve the project.

References

[1] D. S. Dolling, "Fifty years of shock-wave/boundary-layer interaction research: What next?," *AIAA J.*, vol. 39, no. 8, pp. 1517–1531, 2001, doi: 10.2514/2.1476.

[2] A. Ferri, "Experimental results with airfoils tested in the high-speed tunnel at Guidonia," *NACA Tech. Reports*, vol. 946, 1940.

[3] D. Knight, H. Yan, A. G. Panaras, and A. Zheltovodov, "Advances in CFD prediction of shock wave turbulent boundary layer interactions," *Prog. Aerosp. Sci.*, vol. 39, no. 2–3, pp. 121–184, 2003, doi: 10.1016/S0376-0421(02)00069-6.

[4] A. H. Amaha, "Numerical Investigation of Shock wave Turbulent Boundary Layer Interaction over a 2D Compression Ramp," vol. 4, no. 1, pp. 25–32, 2014.

[5] J. Délery and J. P. Dussauge, "Some physical aspects of shock wave/boundary layer interactions," *Shock Waves*, vol. 19, no. 6, pp. 453–468, 2009, doi: 10.1007/s00193-009-0220-z.

[6] G. Andreopoulos, Y., Agui, J. H., and Briassulis, "Shock Wave–Turbulence Interactions," no. 247, pp. 1–6, 2019.

[7] Z. Sun, T. Gan, and Y. Wu, "Shock-wave/boundary-layer interactions at compression ramps studied by high-speed schlieren," *AIAA J.*, vol. 58, no. 4, pp. 1681–1688, 2020, doi:

10.2514/1.J058257.
[8] S. B. Verma, C. Manisankar, and C. Raju, "Control of shock unsteadiness in shock boundary-layer interaction on a compression corner using mechanical vortex generators," *Shock Waves*, vol. 22, no. 4, pp. 327–339, 2012, doi: 10.1007/s00193-012-0369-8.
[9] D. P. Ramaswamy and A. M. Schreyer, "Control of shock-induced separation of a turbulent boundary layer using air-jet vortex generators," *AIAA J.*, vol. 59, no. 3, pp. 927–939, 2021, doi: 10.2514/1.J059674.
[10] A. A. Zheltovodov, "Shock waves/turbulent boundary-layer interactions-fundamental studies and applications," *1996 Fluid Dyn. Conf.*, no. June, pp. 1–27, 1996, doi: 10.2514/6.1996-1977.
[11] W. Hu, S. Hickel, and B. W. Van Oudheusden, "Low-frequency unsteadiness mechanisms in shock wave/turbulent boundary layer interactions over a backward-facing step," *J. Fluid Mech.*, vol. 915, pp. 1–34, 2021, doi: 10.1017/jfm.2021.95.
[12] M. S. Loginov, N. A. Adams, and A. A. Zheltovodov, *Large-eddy simulation of shock-wave/turbulent-boundary-layer interaction*, vol. 565. 2006.
[13] M. Grilli, S. Hickel, and N. A. Adams, "Large-eddy simulation of a supersonic turbulent boundary layer over a compression-expansion ramp," *Int. J. Heat Fluid Flow*, vol. 42, pp. 79–93, 2013, doi: 10.1016/j.ijheatfluidflow.2012.12.006.
[14] D. P. Rizzetta and M. R. Visbal, "Application of Large-Eddy Simulation," vol. 40, no. 8, 2002.
[15] A. J. Smits and K. C. Muck, "Experimental study of three shock wave/turbulent boundary layer interactions," *J. Fluid Mech.*, vol. 182, pp. 291–314, 1987, doi: 10.1017/S0022112087002349.
[16] S. Stolz, N. A. Adams, and L. Kleiser, "The approximate deconvolution model for large-eddy simulation of compressible flows and its application to shock-turbulent-boundary-layer interaction," *Phys. Fluids*, vol. 13, no. 10, pp. 2985–3001, 2001, doi: 10.1063/1.1397277.